American Mineralogist, Volume 79, pages 80–90, 1994

In-situ study of the thermal behavior of cryptomelane by high-voltage and analytical electron microscopy

Paulo Marcos Vasconcelos, Hans-Rudolf Wenk
Department of Geology and Geophysics, University of California, Berkeley, California 94720, U.S.A.
Chuck Echer
National Center for Electron Microscopy, University of California, Lawrence Berkeley Laboratory, Berkeley, California 94720, U.S.A.

Abstract

Scanning electron microscope (SEM) and transmission electron microscope (TEM) studies show that cryptomelane and Cu-rich cryptomelane crystals from weathering profiles in Brazil range from 10 to 200 nm in diameter and have aspect ratios of 1:10 to 1:100 between the short and long dimensions. Acicular crystals identified in hand specimen and in the scanning electron microscope are often composed of bundles of fibers elongated along the **c** axis (tetragonal) or the **b** axis (monoclinic). In-situ heating with a high-voltage transmission electron microscope (HVEM) and an analytical electron microscope (AEM) indicates that upon heating in vacuum cryptomelane crystals begin to transform into a mixed hausmannite and manganosite phase at 648 °C. Mineral transformations are followed by the loss of K from the cryptomelane tunnel sites. Cu-rich cryptomelane transforms into hausmannite between 330 and 515 °C, and manganosite begins to form at 620 °C. Cu-rich cryptomelane also loses K and exsolves native copper upon heating, suggesting that Cu occupies the same site (the A site) as K. Similar mineral transformations are observed when the same samples are heated in air, although the transformations occur at higher temperatures than those observed in vacuum.

The variation in the thermal stability of hollandite-group minerals suggests that the size of A-site occupants may control the mobility of cations along the tunnel direction. Relative grain sizes and the degree of crystallinity of supergene cryptomelane may also influence the thermal stability of hollandite-group minerals. The applicability of cryptomelane and other hollandite-group minerals to K-Ar and $^{40}Ar/^{39}Ar$ dating is discussed in light of the electron microscope investigation results. Ar release from the cryptomelane samples during $^{40}Ar/^{39}Ar$ vacuum laser heating is also discussed in terms of the phase transformations observed by electron microscopy.

Introduction

Recent $^{40}Ar/^{39}Ar$ laser-heating dating has shown that K-bearing manganese oxides (cryptomelane and hollandite) are potentially suitable minerals for dating weathering processes by the K-Ar and $^{40}Ar/^{39}Ar$ methods (Vasconcelos et al., 1992). The ubiquitous presence of these datable oxides in weathering profiles and soils throughout the world may provide information on rates of weathering processes, soil formation, paleoclimates, and landscape evolution. To establish the applicability of cryptomelane to K-Ar and $^{40}Ar/^{39}Ar$ dating it is necessary to define its composition, structure, and range of stability. It is imperative to determine the size range of cryptomelane crystals in order to assess the possibility of ^{39}Ar recoil from the mineral structures during the neutron irradiation procedure required for $^{40}Ar/^{39}Ar$ analysis. In addition, it is necessary to investigate ordering of the tunnel site occupants to determine if cations, H_2O, and the radiogenic ^{40}Ar occupying these sites are easily exchangeable. Finally, in order to interpret the results of $^{40}Ar/^{39}Ar$ experiments better we must understand the thermal behavior of hollandite-group minerals. In particular, the temperature and the mineral transformations associated with the Ar release steps need to be known to determine if cryptomelane retains Ar at normal Earth's surface temperature and to determine that thermal degassing of manganese oxides does not occur during neutron irradiation.

Cryptomelane and hollandite belong to the hollandite group and have the general formula $(A)_{1-2}B_8O_{16}\cdot xH_2O$. The A site can be occupied by large cations such as K^+, Ba^{2+}, Na^+, Cu^+, Pb^{2+}, Rb^{2+}, Sr^{2+}, Cs^{2+}, etc., whereas the $^{[6]}B$ site includes Mn^{3+}, Mn^{4+}, Fe^{3+}, Al^{3+}, Si^{4+}, and Mg^{2+} (Burns and Burns, 1979). Cryptomelane is the K and hollandite is the Ba end-member of a solid-solution series (Byström and Byström, 1950). Byström and Byström (1950) showed that *A* cations occupy a tunnel structure formed by edge-sharing B-O octahedra. Electrostatic

0003–004X/94/0102–0080$02.00

repulsion between the *A* cations requires that the A sites be only partially occupied. Byström and Byström (1950) have proposed that the tunnel cations occupy a special position along the tunnel, which should be 0, ½, 0 in the monoclinic hollandite structure and 0, 0, ½ in the tetragonal cryptomelane structure. Charge-balance requirements indicate that lower valence cations must occupy the B sites to compensate for the presence of the *A* cations (Post et al., 1982; Post and Burnham, 1986; Vicat et al., 1986). Vacancies in the B sites have also been proposed as a charge-balance mechanism (Byström and Byström, 1950). Among the common K-bearing manganese oxides, hollandite is the most promising datable group because of its large range of stability and its occurring as a hypogene phase in hydrothermal environments (Hewett and Fleischer, 1960), as metamorphic minerals in high *P-T* environments (Roy and Purkait, 1965; Miura et al., 1987), and as supergene phases in soils and weathering profiles (Hewett and Fleischer, 1960). In addition, the 2 × 2 tunnel structure of hollandite-group minerals is more likely to retain K and Ar than the more open structures of other K-bearing manganese oxides, such as romanechite (2 × 3 tunnels), todorokite (3 × 3 tunnels), and birnessite (layered structure) (Burns and Burns, 1979; Post and Veblen, 1990).

Thermogravimetric analysis (TGA) and differential-thermal analysis (DTA) of manganese oxides have indicated that dehydration reactions occur at 200–400 °C, and dehydroxylation occurs at higher temperatures (~650 °C) (Kulp and Perfetti, 1950; Ljunggren, 1955). Heating experiments in open air have indicated that cryptomelane transforms into bixbyite at 600 °C, into tetragonal hausmannite at 825 °C, and finally into cubic hausmannite at 1050 (Faulring et al., 1960) or at 1160 °C (Van Hook and Keith, 1958). DTA analyses by Kudo et al. (1990) showed that tetragonal cryptomelane transforms into a monoclinic structure at 710 °C in air and into hausmannite through bixbyite at 850–950 °C.

To investigate the mineralogical and crystallographic relations of supergene potassium manganese oxides, we analyzed cryptomelane samples by powder XRD, electron microprobe (EM), SEM, and TEM. We also monitored phase transformations of two of these samples in situ, with a heating stage in the HVEM. The degassing history of two samples was further studied by laser-heating $^{40}Ar/^{39}Ar$ analysis, and the degassing steps are correlated with the mineralogical transformations observed in the TEM.

Field sites

We investigated hollandite-group minerals from two weathering profiles in Brazil. The first sample, PEG-01 (Table 1), came from deep weathering profiles in the pegmatite fields in the state of Minas Gerais (Vasconcelos et al., 1992). This sample occurs as intimately interconnected botryoidal potassium manganese oxide nodules forming a three-dimensional dendrite-like pattern. During weathering of primary minerals, supergene solutions enriched in K^+ and Mn^{2+} fill open spaces provided by miarolitic cavities in the pegmatites, promoting the precipitation of high-purity cryptomelane inside these cavities. The autocatalytic nature of manganese oxide precipitation leads to the continuous adsorption and subsequent precipitation of dissolved Mn^{2+} onto previously precipitated Mn^{4+}-bearing oxide surfaces, forming concentric growth bands (Fig. 1) (Crerar and Barnes, 1974; Crerar et al., 1972). Backscattered SEM investigation and microprobe analysis showed that differences in the composition of botryoidal growth bands in PEG-01 suggests rhythmic variations in the composition of the weathering solutions (Fig. 1).

Samples F226-121, F40-142, and F115-139.8 (Table 1) came from laterites developed over the Igarapé Bahia hydrothermal Cu-Au deposit in the Carajás Mountains, eastern Amazon (Vasconcelos et al., 1993). The samples occur as massive manganese oxides replacing weathered schists. Randomly oriented manganese oxide crystals have precipitated in the pore spaces around silicate crystals; after dissolution of the silicate matrix, they form a net-

Table 1. Microprobe analyses of manganese oxides

	Monoclinic			Tetragonal
Element	F226-121	F40-142	F115-139.8	PEG-01
Si^{4+}	0.06	0.05	0.03	0.05
Al^{3+}	0.52	0.18	0.08	0.13
Fe^{3+}	0.02	0.01	0.22	0.00
Mn^{4+}	55.05	56.44	56.43	57.57
Co^{2+}	0.25	0.20	0.14	0.00
V^{3+}	0.00	0.00	0.00	0.05
Cu^{+}	2.80	1.51	1.40	0.00
Ca^{2+}	0.11	0.10	0.17	0.12
Na^{+}	0.08	0.13	0.09	0.07
K^{+}	3.01	3.04	2.98	4.91
Ba^{2+}	0.14	0.36	0.01	0.55
Sr^{2+}	0.04	0.14	0.08	0.13
P^{5+}	0.21	0.20	0.24	0.44
O_{meas}	35.29	34.65	34.79	34.75
O_{calc}	34.01	34.37	33.62	35.71
Total	97.58	97.01	96.66	98.77
***B* cations**				
Si^{4+}	0.02	0.01	0.01	0.01
Al^{3+}	0.15	0.05	0.02	0.07
Fe^{3+}	0.00	0.00	0.03	0.00
Mn^{4+}	7.56	7.67	7.66	7.54
Co^{2+}	0.03	0.03	0.02	0.00
V^{3+}	0.00	0.00	0.00	0.01
Total	7.76	7.76	7.74	7.63
***A* cations**				
Cu^{+}	0.33	0.18	0.08	0.00
Ca^{2+}	0.02	0.02	0.03	0.02
Na^{+}	0.03	0.04	0.03	0.02
K^{+}	0.58	0.58	0.57	0.90
Ba^{2+}	0.01	0.02	0.00	0.03
Sr^{2+}	0.00	0.01	0.01	0.01
Total	0.97	0.85	0.72	0.99
P^{5+}	0.05	0.05	0.06	0.10
Total cations	8.78	8.66	8.60	8.72
Molecular Weight	724.92	720.43	717.55	717.56
Calculated S.G.	4.35	4.32		4.31
RB	0.60	0.60	0.60	0.60
RA	1.19	1.21	1.26	1.31
RB/RA	0.50	0.50	0.48	0.46

Note: elemental weight percentages and formulas based on 16 O atoms. S.G. = specific gravity in grams per cubic centimeters.

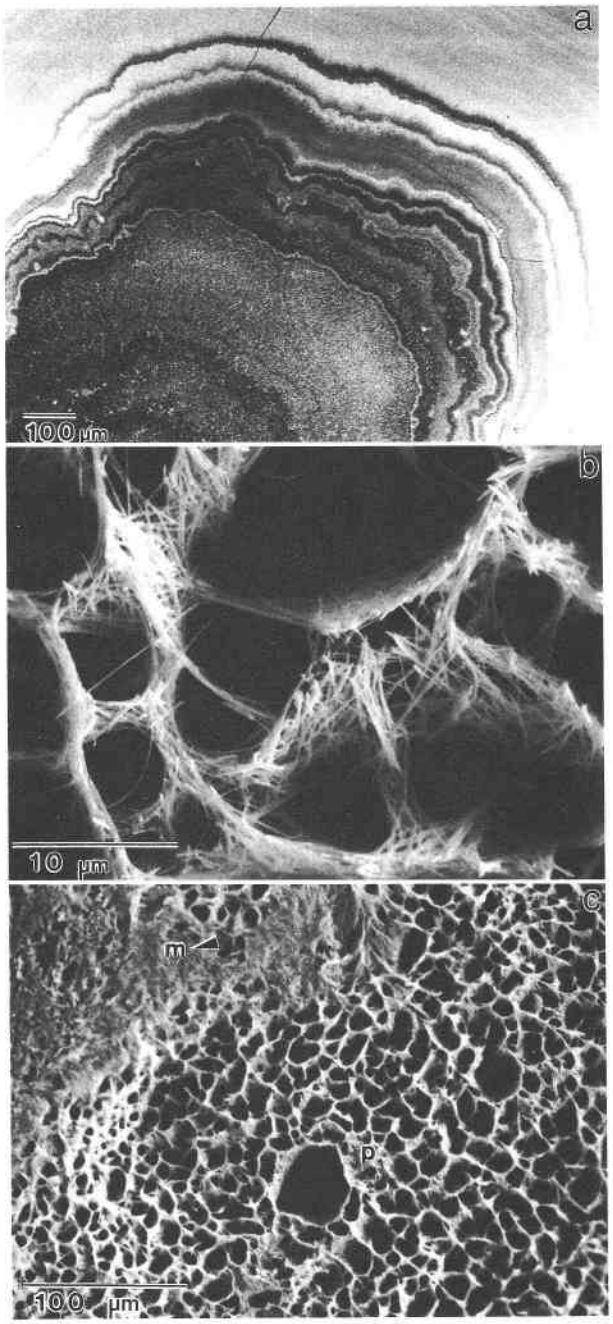

Fig. 1. (**a**) Backscattered SEM photomicrograph of botryoidal cryptomelane (PEG-01); (**b**) SEM photomicrograph of acicular cryptomelane crystals surrounding cavities created by dissolution of silicate grains; (**c**) pseudomorphic (p) texture grading into massive (m) texture as cryptomelane fills cavities previously occupied by silicates.

work of crosscutting needles that preserve the original texture of the host rock (Fig. 1). Further precipitation of manganese oxides in the void spaces creates massive manganese oxide blocks (Fig. 1). K, Ba, and Cu contents in supergene manganese oxides and the absence of these elements from the host schists suggest free mobility of these elements in the weathering solutions. Probable sources of these elements in the weathering solutions are metavolcanic horizons interbedded with the metasediments. The difference in compositions between the Cu-rich samples and the K-rich samples and their distinct degassing behavior during laser-heating $^{40}Ar/^{39}Ar$ analysis (Vasconcelos et al., 1993) made these samples ideally suited for this study.

Experimental methods

The four samples were analyzed using an eight-channel ARL-SEMQ electron microprobe equipped with wavelength-dispersive spectrometers at the Department of Geology and Geophysics at the University of California, Berkeley. The sample current was 30 nA on MgO, the accelerating voltage 15 kV, and the beam diameter 3–5 μm. PEG-01 was also analyzed with a 15-μm beam diameter, but the results are indistinguishable from those obtained with a focused beam.

Powder X-ray diffraction analyses were performed with a Rigaku Geigerflex X-ray diffractometer with Cu$K\alpha$ radiation over the range $3 < 2\theta < 90°$ with scan speeds of 1, 0.5, and 0.25°/min. Measurements of each sample were repeated three to four times, and the average peak positions were calibrated against a Si standard under the same conditions. Unit-cell parameters were calculated using a modified version of the least-squares refinement program LCLS (Burnham, 1962) (Table 2) and confirm all four samples as cryptomelane. Calculations for a body-centered tetragonal unit cell (space group $I4/m$) and a monoclinic unit cell (space group $I2/m$) were carried out for comparison.

After petrographic observations and electron microprobe and scanning electron microscope analysis, suitable thin foils of samples PEG-01 and F226-121 were prepared by ion-beam thinning for study in the heating stage of the Kratos 1.5-MeV HVEM at the National Center for Electron Microscopy (NCEM), Lawrence Berkeley Laboratory. The samples were characterized before heating by a series of selected-area diffraction (SAD) patterns and bright-field photomicrographs. The samples were heated at a rate of 10 °C/min to a maximum T of 848 °C and SAD patterns and bright-field photomicrographs were recorded throughout this process. The temperature within the heating stage was monitored by a Chromel-Alumel thermocouple, and calibration procedures indicated that the temperature readings were within 5 °C from actual sample temperature.

Two foils of sample F226-121 and one foil of PEG-01 were examined in the JEOL 200-kV analytical electron microscope at the NCEM. The AEM has a Kevex EDX detector and corresponding processing facilities, which permitted the variations in composition of the samples before and after heating to be investigated. A beryllium sample holder and grid was employed to obviate spurious X-rays from the holder that might interfere with the sample analysis. The low energy of the 200-kV electrons and

TABLE 2. Unit-cell parameters and structural information of cryptomelane

Space group:	*I*4/*m*	*I*4/*m*	*I*4/*m*
Sample:	PEG-01	F40-142	F226-121
a (Å)	9.846(16)	9.814(24)	9.834(31)
b (Å)	9.846(16)	9.814(24)	9.834(31)
c (Å)	2.860(5)	2.872(9)	2.857(9)
α (°)	90	90	90
β (°)	90	90	90
γ (°)	90	90	90
V (Å^3)	277.24(90)	276.65(136)	276.28(168)
No. of reflections	18	13	10
Specific gravity (calc.)	4.30	4.34	4.38

Note: standard deviations are in parentheses.

the highly condensed beam caused significant damage to sample F226-121, which underwent a phase transformation in the beam. This feature allows mineral transformations induced in the sample by electron beam and heating damage to be investigated and compared with phase transformations observed during external heating. Sample PEG-01 was much more stable in the electron beam, and, in spite of extended investigation, no damage was observed.

Single grains of sample PEG-01 and a Cu-rich cryptomelane sample (F115-139.8) from the Igarapé Bahia profile were further analyzed by $^{40}Ar/^{39}Ar$ analysis (Vasconcelos et al., 1993). Sample preparation and irradiation procedures, experimental conditions, and analytical results were presented in Vasconcelos et al. (1993).

RESULTS

Table 1 shows mineral compositions and site occupancies calculated from the average results of electron microprobe analyses of each sample (592 points analyzed for sample PEG-01, 198 points for sample F226-121, 100 points analyzed for F40-142, and 49 points for F115-139.8). The low totals reported cannot be accounted for by unanalyzed elements. These samples were checked by EDX and WDS scans, and no other elements were present in significant amounts. Previous analyses of cryptomelane by other researchers have indicated that significant amounts of H_2O (1–3.8 wt%) can be present in these supergene oxides (Byström and Byström, 1950; Mathieson and Wadsley, 1950; Perseil and Pinet, 1976; Miura et al., 1987; Ostwald, 1988). We conclude that H_2O is present in the cryptomelane samples analyzed.

The cell occupancy calculations shown in Table 1 suggest that the B site is only partially occupied. In addition, charge-balance considerations (based on 16 O atoms) and the measured O contents suggest that all Mn cations present in the B site are in the Mn^{4+} oxidation state. Previous authors (Byström and Byström, 1950; Burns and Burns, 1979; Miura et al., 1987) have suggested that the charge of *A* cations may be compensated by the presence of vacancies in the B site. In the general formula proposed by Byström and Byström (1950), $A_{2-y}B_{8-z}X_{16}$, *z* varies from 0.1 to 0.5 for the minerals analyzed. Twelve hollandite

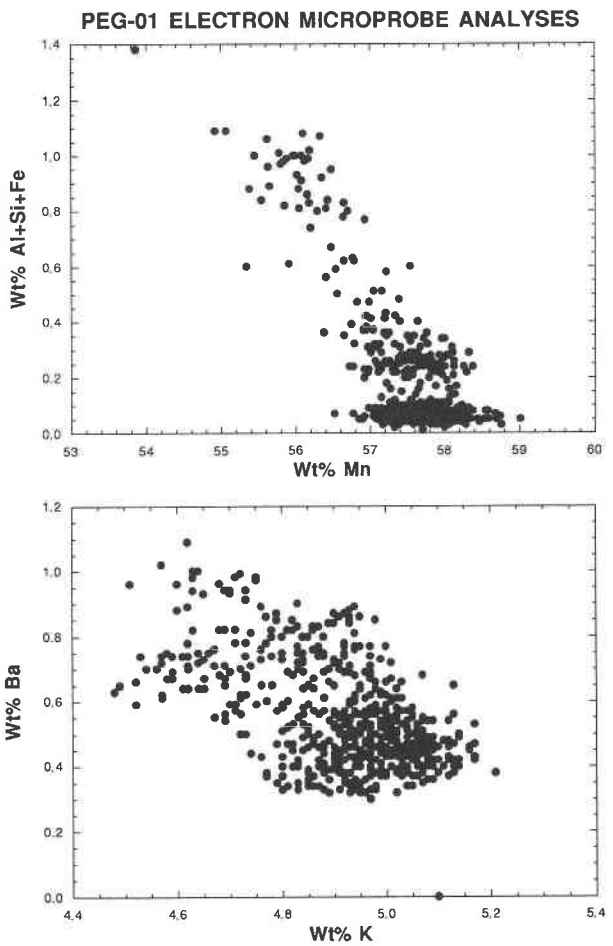

Fig. 2. Elemental correlation from electron microprobe analyses of sample PEG-01.

and 36 cryptomelane samples analyzed by Miura et al. (1987) also showed vacancies in the B site, with *z* ranging from 0.300 to 0.153. These vacancies could allow for charge compensation of the A-site cations and would preclude the necessity for the presence of a lower oxidation state of Mn in the B site.

The Mn contents of the samples analyzed should also decrease with increasing Si, Al, and Fe competition for the octahedral site. Figures 2–4 illustrate the inverse correlation between Mn and Fe + Si + Al contents in the cryptomelane samples analyzed, suggesting competition between Mn and these elements for the B site. Similarly, competition for the tunnel sites may account for the inverse relationship between K and Cu (Fig. 3) and K + Ba + Na + Ca and Cu (Fig. 4). Toledo-Groke et al. (1990), studying Cu-rich cryptomelane from the Salobo profile in Carajás, also noticed evidence for competition between Cu and K for the A sites. Although it is yet not certain whether Cu occupies the tunnel sites or substitutes for Mn in the B sites, the elemental correlations and the behavior of Cu during heating of the Cu-rich cryptome-

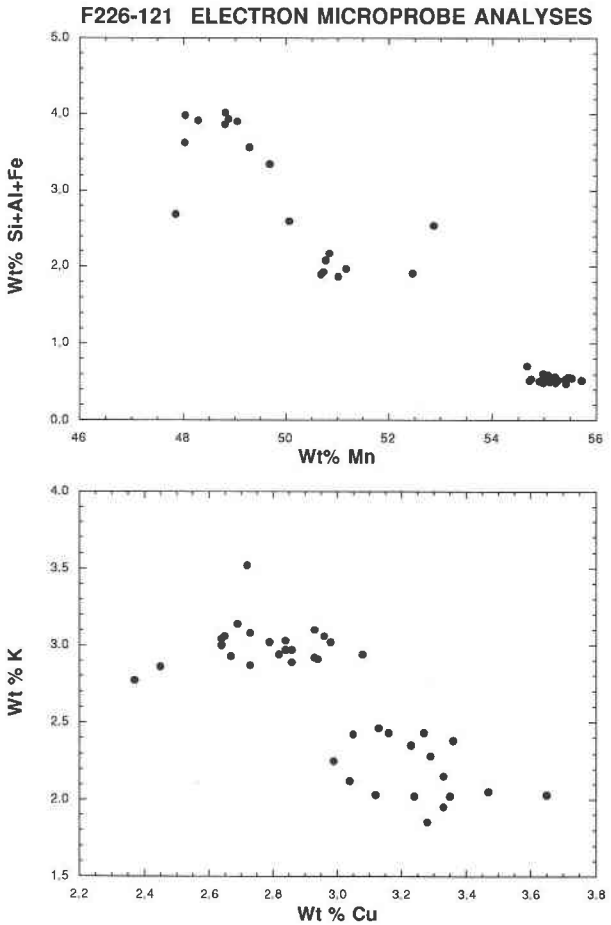

Fig. 3. Elemental correlation from electron microprobe analyses of sample F226-121.

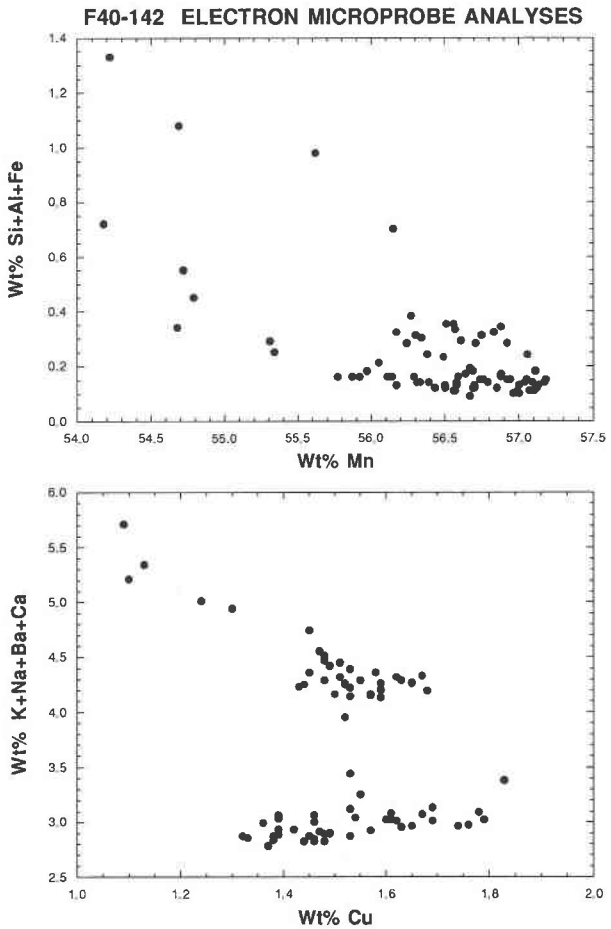

Fig. 4. Elemental correlation from electron microprobe analyses of sample F40-142.

lane samples described below are suggestive of Cu occupation of the tunnel sites. Structural considerations indicate that Cu, if present in the A site, must occur as Cu^{+} ($r_i = 0.96$ Å) and not as the smaller Cu^{2+} ion ($r_i = 0.72$ Å).

The cell-refinement calculations (Table 2) indicate that the cryptomelane samples analyzed are either tetragonal or monoclinic, with β nearly 90°. The powder pattern results refined assuming tetragonal symmetry ($I4/m$) (Table 2) yield lower residuals than when fitted assuming a monoclinic symmetry ($I2/m$). On the other hand, the presence of doublets and triplets in the powder pattern of some samples is suggestive of a lower symmetry than $I4/m$. The resolution of the powder diffractometer is insufficient to positively identify the space group. Another criterion for distinguishing tetragonal from monoclinic cryptomelane is the ratio of the average ionic radius of B-site to A-site occupants (Post et al., 1982; Vicat et al., 1986). When this ratio is >0.48, the structure should be monoclinic. The ratio of average ionic radius of B cations and A cations in the samples studied (Table 1) suggests that sample PEG-01 should be tetragonal and the Cu-rich cryptomelane should be monoclinic.

Bright-field images and SAD patterns for sample PEG-01 are shown in Figure 5. PEG-01 crystals are prismatic and elongated along [001] (Fig. 5). Prism diameters vary from 50 to 1000 nm, and their lengths range from 500 to 10000 nm; these prisms display square and diamond-shaped cross sections (Fig. 5, arrows). Because of the fine-grained nature of the sample, only ring patterns were obtainable by SAD. In order to obtain single-crystal information, convergent beam electron diffraction (CBED) patterns were necessary (Fig. 5). The CBED patterns for PEG-01 crystals indicate that the mineral is possibly tetragonal and elongated along the **c** axis. The CBED pattern in Figure 5 shows the **a*c*** plane of tetragonal cryptomelane or the **a*b*** plane of monoclinic cryptomelane (Fig. 5). It was possible to obtain lattice fringes (Fig. 5). The measured d value of 7.1 Å corresponds to the (110) planes of cryptomelane (Fig. 5). In addition to the 7.1-Å lattice fringes of cryptomelane, some 10-Å lattice fringes were also present. Similar patterns were observed by Turner and Buseck (1979), who interpreted the 10-Å distances as romanechite intergrown with the 7-Å hollandite. Chen et al. (1986) also observed similar lattice

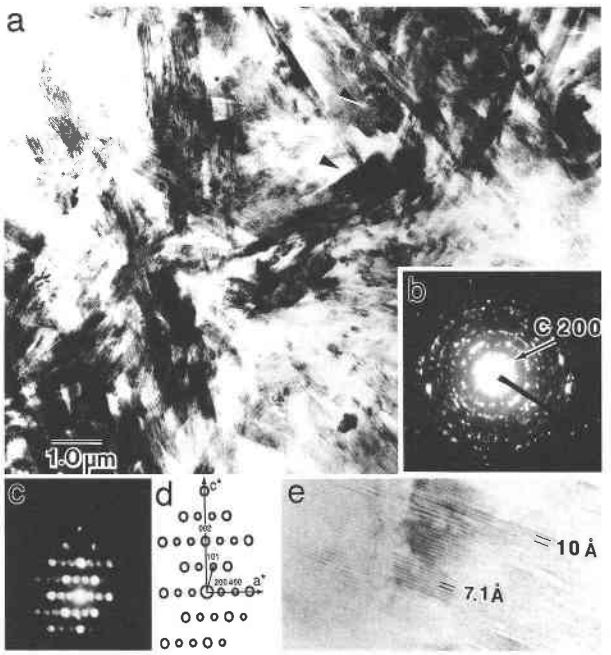

Fig. 5. (**a**) BF image of crosscutting network of cryptomelane crystals in PEG-01. Elongated prismatic and rod-shaped crystals are typical habits for this cryptomelane sample. Arrows show the cross sectional shape of a crystal oriented perpendicularly to the plane of the photograph; (**b**) SAD ring pattern of cryptomelane (see Table 4 for indexed *d* values for ring pattern); (**c**) microbeam diffraction pattern of tetragonal cryptomelane crystals along the **b** axis; (**d**) indexing of SAD pattern shown in **c**; (**e**) TEM image of properly oriented cryptomelane crystals showing predominantly well-ordered 7.1-Å fringes [(110) planes of cryptomelane] and a few 10-Å fringes [possibly (100) planes of psilomelane or (001) planes of todorokite].

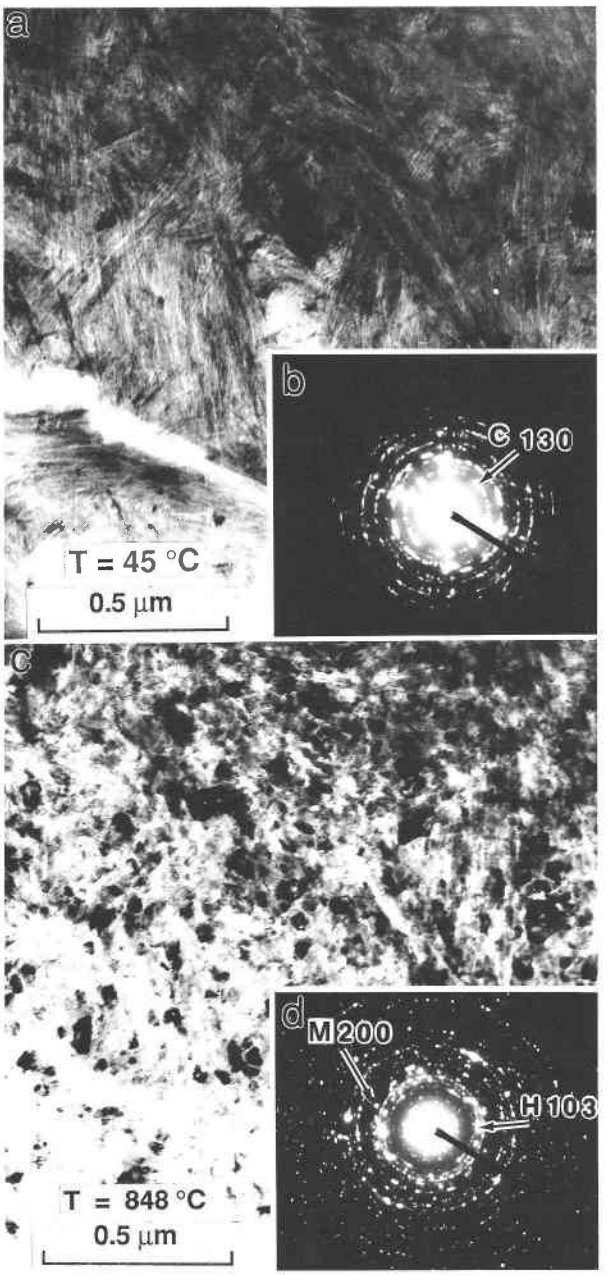

Fig. 6. (**a**) BF image of crosscutting network of cryptomelane needles in sample F226-121 before heat-induced phase transformation; (**b**) SAD ring patterns of cryptomelane crystals; (**c**) BF image of granoblastic texture formed by intergrown hausmannite, manganosite, and dispersed native copper in the sample after heat-induced phase transformation; (**d**) SAD ring pattern of newly formed phases after heat treatment.

irregularities in synthetic cryptomelane crystals formed epitaxially after birnessite.

Bright-field images and SAD ring patterns of sample F226-121 before and after phase transformations are shown in Figure 6. Diffuse SAD ring patterns for sample F226-121 (Fig. 6) indicate that single crystals of cryptomelane are much smaller than the diameter of the electron beam (~1 μm). These cryptomelane crystals are acicular and have diameters ranging from 10 to 120 nm; their lengths may reach 1000 nm.

Mineralogical transformations during heating and electron beam damage

Indexing of SAD patterns taken for the two samples during the heating experiment (Fig. 7 and Table 3 for sample F226-121 and Figure 8 and Table 3 for sample PEG-01) indicated that the two samples exhibit slightly different behaviors during the HVEM heating experiments. The fibrous and prismatic cryptomelane crystals in the K-rich sample (PEG-01) were surprisingly resistant to phase transformations, persisting in vacuum up to T = 648 °C (Fig. 8 and Table 3). The Cu-rich sample (F226-121) (Fig. 7 and Table 3) underwent phase transformations at lower temperatures, as indicated by the almost complete disappearance of the cryptomelane lines in the SAD pattern for the sample at T = 620 °C.

Both samples underwent sudden phase transformations during in-situ heating investigations, but not all

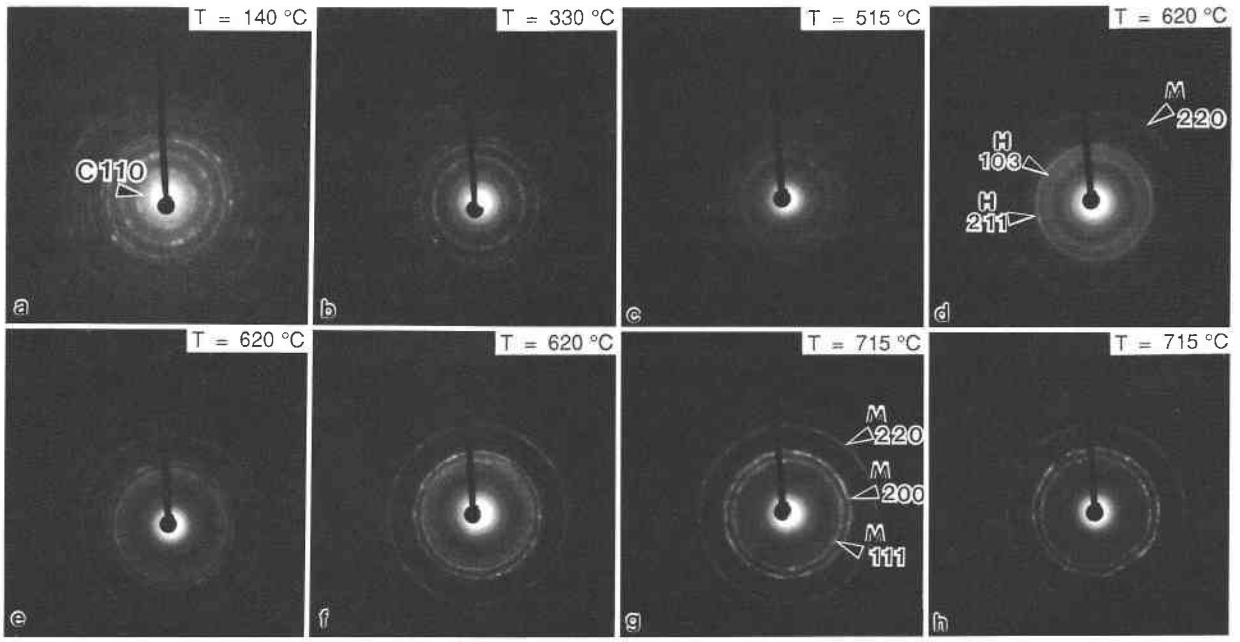

Fig. 7. (**a–h**) SAD ring patterns depicting mineral transformations in sample F226-121 during in-situ HVEM heating. Mineral parageneses are summarized in Table 3. Temperature and some diagnostic reflections are indicated. C = cryptomelane; H = hausmannite; M = manganosite. Several diffraction patterns were taken at the same temperature (**d–f** and **g–h**). Note that at 620 °C hausmannite disappears during prolonged heating and manganosite becomes the dominating phase.

crystals underwent transformation at the same time. The difference in behavior between the two samples and the different behavior of cryptomelane crystals in a single sample suggest that small differences in composition between cryptomelane crystals possibly accelerate or retard the transition from low- to high-temperature phases. In addition, other factors, such as grain size, crystal morphology and orientation, surface properties, and kinetic

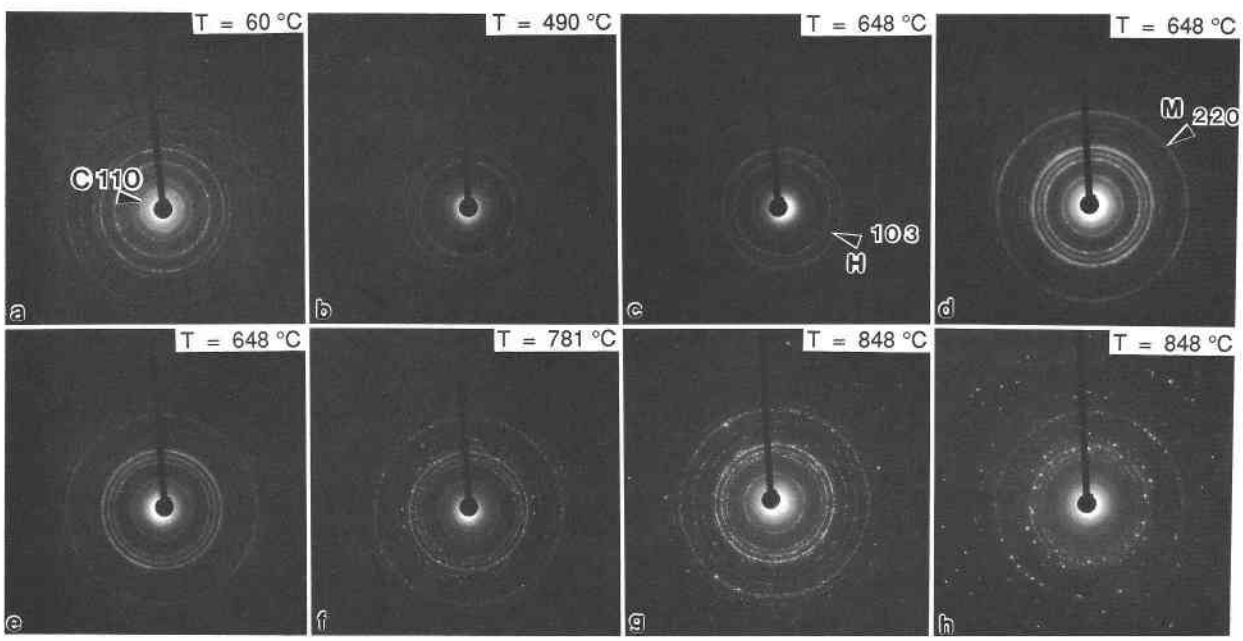

Fig. 8. (**a–h**) SAD ring patterns illustrating mineral transformations in sample PEG-01 during in-situ HVEM heating. Mineral parageneses are shown in Table 3. Temperature and some diagnostic reflections are indicated. C = cryptomelane; H = hausmannite; M = manganosite. At 648 °C (**c**) hausmannite crystallizes and later transforms to manganosite (**e**). Notice coarsening at 848 °C as continuous rings (**g**) change to a spot pattern (**h**).

TABLE 3. Mineral paragenesis during heating in HVEM

Sample F226-121							
140 °C	330 °C	515 °C	620 °C	620 °C	620 °C	715 °C	715 °C
C(+)	C(+)	B(−) H(+) C	H(+) M(−)	H(+) M	M(+) H(−)	M(+) H(−)	M(+) H(−)
Sample PEG-01							
60 °C	490 °C	648 °C	648 °C	648 °C	781 °C	848 °C	
C(+)	C(+)	C H	H(+) C M	H(+) M C	H M	M(+) H(−)	

Note: C = cryptomelane, B = bixbyite, H = hausmannite, M = manganosite; + = abundant, − = minor.

constraints, may also retard the phase transitions observed and must be evaluated.

During heating with a heating stage, the Cu-rich cryptomelane sample transformed to hausmannite and native copper. Hausmannite crystals are coarser grained than the starting cryptomelane needles (Fig. 6b). As the phase transformations progressed, the crosscutting network of acicular cryptomelane crystals (Fig. 6a) was progressively replaced by a granoblastic texture (Fig. 6b), in which coarser grained idiomorphic crystals of hausmannite and manganosite are joined at 120° angles and native copper grains, <0.005 μm, occur dispersed throughout the sample. Textural evolution of the samples during heating suggests that crystals oriented perpendicularly to the sample surface recrystallize more readily than the crystals oriented parallel to it (Fig. 6, arrow). This observation is consistent with recrystallization by breakdown of the tunnel structure due to migration of A cations out of the tunnel sites. Electron beam damage produced phase transformations similar to external heating (Fig. 9b). Hausmannite and native copper suddenly crystallized during cryptomelane breakdown (Fig. 9b). It is possible that the temperatures reached in the electron beam were high enough to promote the phase transformations observed.

EDX semiquantitative analysis of sample F226-121 before and after phase transformation by electron beam damage showed the loss of K and Cu from the manganese oxide structures as it transformed from cryptomelane to hausmannite. The loss of these elements was accompanied by a relative enrichment in Al and Co, whereas Mn remained relatively unaffected. This is interpreted as ev-

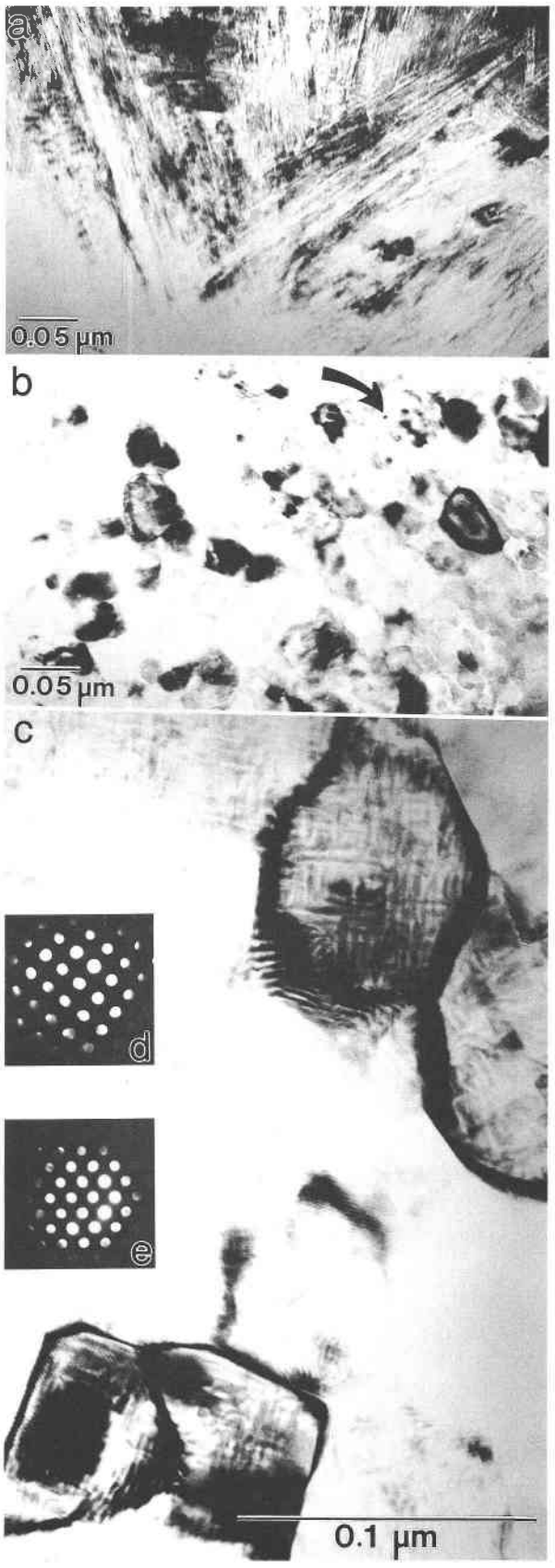

→

Fig. 9. (**a**) BF image of crosscutting network of cryptomelane needles in sample F226-121 before phase transformation induced by electron beam; (**b**) BF image of granoblastic texture formed by intergrown hausmannite, manganosite, and dispersed native copper in the sample (arrow) after phase transformation induced by electron beam; (**c**) BF image of sample F226-121 showing granoblastic texture and single-crystal microbeam diffraction patterns of the newly formed hausmannite (**d**) and manganosite (**e**) crystals.

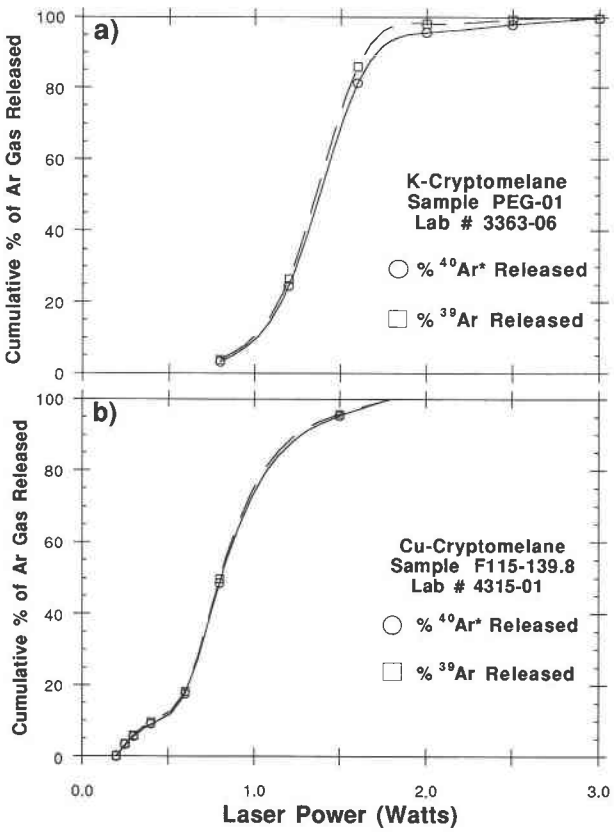

Fig. 10. (**a**) Release of Ar isotopes during laser-heating $^{40}Ar/^{39}Ar$ analysis of sample PEG-01; (**b**) Release of Ar isotopes during laser-heating $^{40}Ar/^{39}Ar$ analysis of sample F115-139.8. The curve in **a** indicates that the K-rich cryptomelane sample releases its radiogenic $^{40}Ar^*$ and nucleogenic ^{39}Ar at a narrow range of laser power. The Cu-rich cryptomelane sample (**b**) also releases its $^{40}Ar^*$ and ^{39}Ar isotopes at a narrow range of laser power, but less laser energy is required to degas the Cu-rich sample.

idence for the presence of Al and Co in the octahedral sites; the octahedral sites undergo structural rearrangement but remain otherwise undisturbed during the phase transformation. The loss of K and Cu is attributed to the breakdown of the tunnel structure. K and Cu are exsolved from the tunnel site; Cu forms a distinct phase (native copper) (Fig. 9b), and K is lost by volatilization. Native copper has also been found as a residue together with manganosite in samples fused for K-Ar analysis and in samples heated in a furnace to 900 °C, further strengthening this hypothesis.

Hausmannite forms euhedral cube-shaped crystals (Fig. 9b, 9c). Indexed SAD ring patterns (Figs. 7, 8, and 9) and microbeam single-crystal diffraction patterns (Fig. 9d) suggest a tetragonal crystal lattice for hausmannite. The noticeable presence of a tweed structure (Fig. 9c) in hausmannite crystals may be attributed to the distortion of the crystal structure during the phase transformation from a high-temperature cubic spinel structure into the lower temperature tetragonal hausmannite structure (space group $I4_1$) (Frenzel, 1980). Although under normal pressure conditions the tetragonal-cubic phase transformation in hausmannite occurs between 1050 and 1160 °C, it is possible that in vacuum this transformation may occur below 848 °C. Another explanation for the modulated structure is an incipient chemical fluctuation. SAD ring patterns (Figs. 6, 8, 9) and microbeam diffraction patterns (Fig. 9e) also show the presence of manganosite crystals after the heating of cryptomelane crystals in vacuum.

Laser-heating $^{40}Ar/^{39}Ar$ results

The Ar release history of the K-rich and the Cu-rich cryptomelane samples are shown in Figure 10. The degassing history of the two samples is remarkably similar; most of the radiogenic $^{40}Ar^*$ and nucleogenic ^{39}Ar fractions are released at a narrow range of laser power. Despite the similarities in the Ar degassing patterns for the two samples, the K-rich sample requires a higher laser energy output to release its Ar gas. This difference in degassing history may be accounted for by different coupling between each sample and the laser beam. Another possible explanation is that the K-rich sample undergoes phase transformation at a higher temperature than the Cu-rich sample. The laser-heating $^{40}Ar/^{39}Ar$ experiment also shows a close similarity between the $^{40}Ar^*$ and ^{39}Ar release curves (Fig. 10), which suggests that these isotopes have the same activation energy, i.e., they occupy the same site in the crystal structure. This is indirect yet strong evidence that significant amounts of ^{39}Ar are not displaced by recoil out of the tunnel sites.

Discussion

The investigation of supergene manganese oxides at the appropriate scale and with the proper methodology suggests that the oxides we studied are, on the whole, well-crystallized single minerals with only minor occurrences of other intergrown phases. The high degree of crystallinity and the purity of these minerals, in spite of their extremely fine-grained nature, suggest that they should be suitable for radiometric dating, provided that ^{40}Ar and K do not easily diffuse into and out of the mineral structures and that ^{39}Ar recoil loss does not occur.

The diffusion of K from cryptomelane structures was studied by electrodialysis (Sreenivas and Roy, 1961). These authors proposed that the large tunnel structure, *A* cation disordering, and partial occupancy of the channel sites led to low activation energies for the *A* cations, resulting in a high cation-exchange capacity for these minerals. High cation exchange would also imply loss of K and radiogenic $^{40}Ar^*$, leading to inconclusive dating results. On the other hand, Vicat et al. (1986) interpreted the presence of a superstructure along the **c** axis in synthetic barium titanium hollandite as evidence of ordering of the tunnel *A* cations. This superstructure involves the tripling of the cell along the **c** axis, which Vicat et al. (1986) interpreted as one-dimensional ordering of K cations in the partially filled A sites, following the sequence

K-K-□-K-K-□. Ordering of the *A* cations implies restricted mobility of the cations along the tunnel direction, an important feature for the K and Ar retentivity of hollandite-group minerals. Restricted mobility of *A* cations has also been proposed by Sinclair et al. (1980), who noticed the presence of square-shaped bottlenecks along the channels. These bottlenecks restrict cation motion and explain the high resistance to leaching presented by hollandite-type structures (Sinclair et al., 1980). Cation mobility along the tunnel structure must be a function of the cation radius, and one should expect greater mobility and lower activation energy for smaller cations occupying the A sites. Some authors (Sinclair et al., 1980; Post et al., 1982; Vicat et al., 1986) have shown that some of the *A* cations are displaced from the special position in cryptomelane. Vicat et al. (1986) proposed that K is shifted 0.125 × c away from the 00½ position. Post et al. (1982) have shown that the smaller cations (Na and Sr) form shorter A-O contacts and will be displaced from the (000) position occupied by K. Structural energy calculations also show that smaller tunnel cations are displaced farther from the special positions than larger cations (Post and Burnham, 1986). The model calculations also indicate that the energy minimum calculated for smaller cations is broader and shallower than for larger cations, suggesting that the smaller cations have larger temperature factors (Post and Burnham, 1986). The in-situ mineral transformations observed above suggest that K-rich cryptomelane are more thermally stable than Cu-rich cryptomelane, consistent with the prediction of a larger activation energy for larger cations occupying the A site.

Ar diffusion from mineral structures is controlled by the energy required to distort neighboring atoms and to allow passage of Ar (McDougall and Harrison, 1988). The large atomic radius of Ar (R = 1.96 Å) imposes structural constraints in the tunnel site that impede the migration of Ar out of these sites unless the other A-site occupants (K, Ba, Na, Cu, etc.) are also dislocated. This process will promote the collapse of the hollandite tunnel structure and will favor the formation of bixbyite, hausmannite, and manganosite. The heating-stage EM experiments suggest that K loss and possibly Ar degassing from the fine-grained network of cryptomelane crystals occur by the breakdown of individual needles or fibers. This postulated Ar degassing mechanism differs from volume diffusion models postulated for Ar loss from other mineral structures (McDougall and Harrison, 1988) and is similar to the mechanisms proposed for Ar release from biotite and amphibole by Gaber et al. (1988).

The laser-heating experiments have shown that, in spite of a similar behavior between the K-rich and the Cu-rich cryptomelane samples, these samples release their tunnel-site Ar components at different laser power levels, which most probably indicates degassing at different temperatures. These results are consistent with the observation that samples richer in small cations in the tunnel sites (Cu-rich samples) undergo phase transformations more readily than samples rich in large cations in the A site.

Conclusions

The range of crystal sizes observed by electron microscopy indicates that the supergene manganese oxides studied, even the well-crystallized ones, are very fine grained (crystal diameters are generally smaller than 1 μm). In-situ observation of mineral transformations during heating of supergene manganese oxides suggests that these phases have a broad range of thermal stability, even in vacuum. The large range of thermal stability of cryptomelane in vacuum suggests that the mobility of the *A* cation is fairly restricted and requires a large activation energy. The refractory nature of the cryptomelane crystals during in-situ heating-stage experiments also suggests that cryptomelane should not be affected by the temperatures reached inside the nuclear reactor during neutron irradiation ($T \sim 180$ °C).

We postulate that the temperature required for the mineral transformations observed in the TEM, cryptomelane → hausmannite → manganosite, correspond to the temperatures in which radiogenic and nucleogenic Ar isotopes are released from the mineral structures. This indicates that Ar release by hollandite-group minerals is not a volume diffusion phenomena. The identical degassing patterns for radiogenic $^{40}Ar^*$ and nucleogenic ^{39}Ar observed in the laser-heating $^{40}Ar/^{39}Ar$ experiments suggest that these isotopes occupy the same site in the crystal lattice and that ^{39}Ar does not recoil out of the tunnel sites during neutron irradiation in any significant quantities. The very fine-grained nature of the samples studied, on the other hand, suggests that ^{39}Ar recoil is theoretically possible and should be monitored in future experiments.

Acknowledgments

We acknowledge the support of the Brazilian Research Council (CNPq) to P.V. (grant 200392/88-3/GL) and of the National Science Foundation to R.W. (grant EAR-91-04605). We also are thankful for the access to the facilities of the NCEM and the help with the HVEM provided by Doug Owen. We gratefully acknowledge John Donovan for helping with the electron microprobe analysis, Tim Teage for sample preparation, and Ron Wilson for helping with the SEM studies. This project has also benefited from discussions with Tim Becker, Garniss Curtis, and Paul Renne. We also thank the *garimpeiro* Orílio Vaz de Aguilar from Divino das Laranjeiras for help with the collection of manganese oxide samples from pegmatites, and the staff of CVRD mining company, in particular Augusto Kishida, Jose Luzimar do Rego, and Paulo Sergio, for their help and field support. The final manuscript also benefited from insightful comments and suggestions by J. Post and D. Veblen.

References cited

Burnham, C.W. (1962) Lattice constant refinement. Carnegie Institute of Washington Year Book, 61, 132–135.

Burns, R.G., and Burns, V.M. (1979) Manganese oxides. Mineralogical Society of America Reviews in Mineralogy, 6, 1–46.

Byström, A., and Byström, A.M. (1950) The crystal structure of hollandite, the related manganese oxide minerals, and α-MnO_2. Acta Crystallographica, 3, 146–154.

Chen, C.C., Golden, D.C., and Dixon, J.B. (1986) Transformation of synthetic birnessite to cryptomelane: An electron microscope study. Clays and Clay Minerals, 34, 565–571.

Crerar, D.A., and Barnes, H.L. (1974) Deposition of deep-sea manganese nodules. Geochimica et Cosmochimica Acta, 38, 279–300.

Crerar, D.A., Cormick, R.K., and Barnes, H.L. (1972) Organic controls

on the sedimentary geochemistry of manganese. Acta Mineralogica-Petrographica, 20, 217–226.

Faulring, G.M., Zwicker, W.K., and Forgeng, W.D. (1960) Thermal transformations and properties of cryptomelane. American Mineralogist, 45, 946–959.

Frenzel, G. (1980) The manganese ore minerals. In I.M. Varentsov and G. Grasselly, Eds., Geology and geochemistry of manganese, p. 25–158. E. Schweizerbart'sche Verlagsbuchhandlung, Stuttgart, Germany.

Gaber, L.J., Foland, K.A., and Corbató, C.E. (1988) On the significance of argon release from biotite and amphibole during $^{40}Ar/^{39}Ar$ vacuum heating. Geochimica et Cosmochimica Acta, 52, 2457–2465.

Hewett, D.F., and Fleischer, M. (1960) Deposits of the manganese oxides. Economic Geology, 55, 1–55.

Kudo, H., Miura, H., and Hariya, Y. (1990) Tetragonal-monoclinic transformation of cryptomelane at high temperature. Mineralogical Journal, 15, 50–63.

Kulp, J.L., and Perfetti, J.N. (1950) Thermal study of some manganese oxide minerals. Mineralogical Magazine, 29, 239–251.

Ljunggren, P. (1955) Differential thermal analysis and x-ray examination of Fe and Mn bog ores. Geologiska Föreningens iStockholm Förhandlingar, 77/2, 135–147.

Mathieson, A.M., and Wadsley, A.D. (1950) The crystal structure of cryptomelane. American Mineralogist, 35, 99–101.

McDougall, I., and Harrison, T.M. (1988) Geochronology and thermochronology by the $^{40}Ar/^{39}Ar$ method: Oxford monographs on geology and geophysics, 212 p. Oxford University Press, New York.

Miura, H., Banerjee, H., Hariya, Y., and Dasgupta, S. (1987) Hollandite and cryptomelane in the manganese oxide deposits of the Sausar Group, India. Mineralogical Journal, 13, 424–433.

Ostwald, J. (1988) Mineralogy of the Groote Eylandt manganese oxides: A review. Ore Geology Review, 4, 3–45.

Perseil, E.A., and Pinet, M. (1976) Contribution à la connaissance des romanéchites et des cryptomélanes-coronadites-hollandites: Traits essentiels et paragenèses. Contributions to Mineralogy and Petrology, 55, 191–204.

Post, J.E., and Burnham, C.W. (1986) Modeling tunnel-cation displacements in hollandites using structure-energy calculations. American Mineralogist, 71, 1178–1185.

Post, J.E., and Veblen, D.R. (1990) Crystal structure determinations of synthetic sodium, magnesium, and potassium birnessite using TEM and the Rietveld method. American Mineralogist, 75, 477–489.

Post, J.E., Von Dreele, R.B., and Buseck, P.R. (1982) Symmetry and cation displacements in hollandites: Structure refinements of hollandite, cryptomelane and priderite. Acta Crystallographica, B38, 1056–1065.

Roy, S., and Purkait, P.K. (1965) Stability relations of manganese oxide minerals in metamorphic orebodies corresponding to sillimanite grade in Gowari Wadhona Mine Area, Chindwara District, Madhya Pradesh, India. Economic Geology, 60, 601–613.

Sinclair, W., McLaughlin, G.M., and Ringwood, A.E. (1980) The structure and chemistry of a barium titanate hollandite-type phase. Acta Crystallographica, B36, 2913–2918.

Sreenivas, B.L., and Roy, R. (1961) Observations on cation exchange in some manganese minerals by electrodialysis. Economic Geology, 56, 198–203.

Toledo-Groke, M.C., Melfi, A.J., and Parisot, J.C. (1990) Criptomelana cuprífera formada durante o intemperismo das rochas da jazida de cobre do Salobo 3a, Serra dos Carajás. Revista do Instituto Geológico, 11, 35–42.

Turner, S., and Buseck, P.R. (1979) Manganese oxide structures and their intergrowths. Science, 203, 1024–1027.

Van Hook, H.J., and Keith, M.L. (1958) The system Fe_3O_4-Mn_3O_4. American Mineralogist, 43, 69–83.

Vasconcelos, P.M., Becker, T.A., Renne, P.R., and Brimhall, G.H. (1992) Age and duration of weathering by ^{40}K-^{40}Ar and ^{40}Ar-^{39}Ar analysis of K-Mn oxides. Science, 258, 451.

——— (1993) Direct dating of weathering phenomena by ^{40}K-^{40}Ar and ^{40}Ar-^{39}Ar analysis of supergene K-Mn oxides. Geochimica et Cosmochimica Acta, in press.

Vicat, J., Fanchon, E., Strobel, P., and Qui, D.T. (1986) The structure of $K_{1.33}Mn_8O_{16}$ and cation ordering in hollandite-type structures. Acta Crystallographica, B42, 162–167.

Manuscript received February 4, 1993
Manuscript accepted September 20, 1993